HAL
open science

Robust numerical schemes for Eulerian spray DNS and LES in two-phase turbulent flows

Matthieu Boileau, Christophe Chalons, Jean-François Bourgouin, Cédric Terrier, Frédérique Laurent, Stéphane de Chaisemartin, Marc Massot

To cite this version:

Matthieu Boileau, Christophe Chalons, Jean-François Bourgouin, Cédric Terrier, Frédérique Laurent, et al.. Robust numerical schemes for Eulerian spray DNS and LES in two-phase turbulent flows. 7th International Conference on Multiphase Flows, ICMF 2010, May 2010, Tampa, FL, United States. pp.1-15. hal-00498182

HAL Id: hal-00498182

https://hal.science/hal-00498182v1

Submitted on 6 Jul 2010

HAL is a multi-disciplinary open access archive for the deposit and dissemination of scientific research documents, whether they are published or not. The documents may come from teaching and research institutions in France or abroad, or from public or private research centers.

L'archive ouverte pluridisciplinaire **HAL**, est destinée au dépôt et à la diffusion de documents scientifiques de niveau recherche, publiés ou non, émanant des établissements d'enseignement et de recherche français ou étrangers, des laboratoires publics ou privés.

7th International Conference on Multiphase Flow,
ICMF 2010, Tampa, FL, May 30 – June 4, 2010

Robust numerical schemes for Eulerian spray DNS and LES in two-phase turbulent flows

M. Boileau*, C. Chalons†*, J.-F. Bourgouin*, C. Terrier*, F. Laurent*,

S. de Chaisemartin‡ and M. Massot*

* Laboratoire EM2C-UPR CNRS 288, Ecole Centrale Paris, 92295 Châtenay-Malabry, France

† DEN/DANS/DM2S/SFME/LETR CEA-Saclay, 91191 Gif-sur-Yvette, France

‡ Institut Français du pétrole, 92852 Rueil Malmaison, France

matthieu.boileau@em2c.ecp.fr, chalons@math.jussieu.fr, frederique.laurent@em2c.ecp.fr,

stephane.de-chaisemartin@ifp.fr and marc.massot@em2c.ecp.fr (corresponding author)

Keywords: Liquid Sprays; Multi-Fluid models; Spray Equation; Large Eddy Simulation; Relaxation schemes

Abstract

Large Eddy Simulation (LES) and Direct numerical Simulation (DNS) of polydisperse evaporating sprays with Eulerian models are very promising tools for high performance computing of combustion applications. They are able to describe the turbulent dispersion and evaporation and properly predict the combustion regimes. However, the spray system of conservation equations has a convective part which is either similar to gas dynamics Euler equations with a real gas type state law or to the pressureless gas dynamics (PGD), depending on the local flow regime and droplet Stokes number; so, they usually involve singularities due to model closure assumptions and require dedicated numerical schemes. Besides, it is desirable to cope with exactly zero droplet density in some zones of the flow, especially near the injection zone, where droplets are injected in only some spatial locations. Even if the issue has been successfully tackled in de Chaisemartin (2009); Fréret et al. (2010) in the framework of PGD with the use of accurate kinetic schemes, it cannot be directly extended to general gas dynamics. The purpose of the present contribution is to introduce a new generation of numerical methods based on relaxation schemes which are able to treat both PGD and general gas dynamics, as well as to cope in a robust manner with vacuum zones and natural singularities of the resulting system of conservation equations. The proposed hybrid relaxation scheme and algorithms are validated through comparisons with analytical solutions and other numerical strategies on 1D and 2D configurations. They exhibit a very robust behavior and are a very promising candidate for more complex applications since they provide solutions to key numerical issues of the actual Eulerian spray DNS and LES models.

Introduction

Many industrial devices involve turbulent combustion of a liquid fuel. The transportation sector, rocket, aircraft or car engines are almost exclusively based on storage and injection of a liquid phase, which is sprayed into a combustion chamber. It is of primary importance to understand and control the physical process as a whole, from the injection into the chamber up to the combustion phenomena. Numerical simulation is now a standard industrial tool to optimize the turbulent combustion process in such devices (Duchaine et al. (2009)). Thanks to LES, unsteady phenomena such as jet ignition (Lacaze et al. (2009)) or combustion instabilities (Selle et al. (2006); Roux et al. (2008)) can now be accurately predicted in simplified configurations where purely gaseous flames are encountered. Nevertheless, the liquid fuel injection needs special attention in order to properly predict the combustion regimes. It consists in two parts. The first one is related to the atomization process near the injector and requires dedicated models and methods. The second part is related to the spray dynamics once the liquid has reached the structure of a polydisperse cloud of droplets; some promising advances have been performed in the field of spray combustion in real devices (Boileau et al. (2008a,b); Vié et al. (2010)). However, the reliable prediction of such complex two-phase reacting

flows requires further work in the modeling of the triple spray/turbulence/combustion interaction. In particular, the description of the turbulent spray dispersion remains a challenging issue. Spray models have a common basis at the mesoscopic level under the form of a number density function (NDF) satisfying a Boltzmann type equation, the so-called Williams equation (Williams (1958)). The internal variables characterizing one droplet are the size, the velocity and the temperature, so that the total phase space is usually high-dimensional. Such a transport equation describes the evolution of the NDF of the spray due to convection, heating, evaporation and drag force from the gaseous phase and droplet-droplet interactions. Different strategies can be used to solve the dispersed phase dynamics. A first choice is to approximate the NDF by a sample of discrete numerical parcels of particles through a Lagrangian–Monte-Carlo approach (see O'Rourke (1981)). It is called Direct Simulation Monte-Carlo method (DSMC) by Bird (1994) and generally considered to be the most accurate for solving Williams equation; it is especially suited for DNS since it does not introduce any numerical diffusion, the particle trajectories being exactly solved. This approach has been widely used and has been shown to be efficient in numerous cases. Its main drawback is the delicate coupling between the Lagrangian description of the dispersed phase and the Eulerian description for the gaseous phase. Moreover, from a computational point of view, a Lagrangian solver is difficult to efficiently parallelize using the domain decomposition used by the gas solver. This is particularly true in massively parallel calculations where only a few parallel blocks may contain most of the Lagrangian particles and need dedicated algorithms as in Garcia (2009). Finally, unsteady computations of polydisperse sprays require a large number of parcels in each Eulerian cell, leading to large memory needs and high CPU costs. As a consequence, as long as it is able to describe the essential feature of polydispersity, an Eulerian formulation for the dispersed phase is more attractive for massively parallel simulations of industrial configurations.

Based on the ideas of Greenberg et al. (1993) and following the work of Laurent and Massot (2001), de Chaisemartin (2009) have developed a multi-dimensional Eulerian Multi-Fluid solver capable of describing the polydispersity of a spray in size and the associated size-conditioned dynamics. This approach relies on the derivation of a semi-kinetic model from the Williams equation using a moment method for velocity conditioned by droplet size while keeping the continuous size distribution function. The key issue is in the velocity moment closure for which two strategies exist. The first one, based on the quadrature method (see Kah et al. (2010) and references therein), has been developed to capture strongly non equilibrium velocity distributions and will not be treated in the present contribution. The second one, adopted in the present paper, is based on equilibrium velocity distributions either with zero dispersion around the mean in the framework of DNS such as in de Chaisemartin (2009); Fréret et al. (2010) and references therein or with non-zero dispersion in the framework of ensemble averages and modeling non-resolved scales such as in Massot et al. (2004); Massot (2007) and Vié et al. (2010).

In the context of spray dynamics, a zero pressure assumption means that the probability density function of particle velocity is a Dirac in the velocity space, i.e. that no dispersion in the local instantaneous particle velocity is considered. For this assumption to be true, the relaxation time of particles must not exceed the timescale of the fluid turbulence. Otherwise, the effect of trajectory crossing due to higher-inertia particles induces a random-uncorrelated component of particle motion that must be taken into account. Simonin et al. (2002) and Kaufmann et al. (2008) proposed a formalism that account for this random-uncorrelated motion in the context of DNS. Moreau et al. (2005) and Riber et al. (2005, 2009) have extended this approach for LES. They used a spatial filtering of Kaufmann's system of Eulerian conservation equations and proposed a model for the resulting particulate subgrid stresses. Another way to use the LES concept for the spray equations is to apply the spatial filtering directly to the Williams equation for the PDF of particle velocity (see Pandya and Mashayek (2002) and Zaichik et al. (2009)). The resulting kinetic equation for the filtered PDF has the same form as the statistical PDF equation initially derived by Reeks (1992) in the context of RANS and used in Massot et al. (2004). Whatever the approach for turbulence modelling (DNS, LES or RANS) and the level of corresponding filtering (on the kinetic equation or on the moment equations at the semi-kinetic level), the local velocity dispersion of particles introduces stress, and more specifically a pressure-like term, in the spray conservation equations. Finally, the Eulerian equations for inertial particles dynamics are similar to the gas dynamics equations. In particular, they include a real gas type state law which can eventually degenerate in some parts of the flow to a zero pressure term leading to the peculiar PGD. Let us emphasize that the size distribution function is then discretized using a finite volume approach in the size phase space that yields conservation equations for mass, momentum (and eventually other properties such as enthalpy) of droplets in fixed size intervals which have the same mathematical structure. In the present paper, we will consider a monodisperse spray so that the semi-kinetic model is sufficient, keeping in mind that all the developed tools can be easily extended to poly-

dispersity in the framework of the multi-fluid method de Chaisemartin (2009); Vié et al. (2010).

The main difficulty of the resulting system of conservation equations is related to transport in physical space, that is the convective part of the system, which is either hyperbolic or weakly hyperbolic, and thus leads to singularity formation. In the framework of the PGD system, de Chaisemartin (2009) has solved the problem by using a numerical strategy based on the kinetic scheme of Bouchut et al. (2003) which leads to a second order method in space and time with very limited diffusion. This numerical scheme makes it possible to capture accurately the delta-shocks in density and vacuum states which naturally emerge from the weakly hyperbolic system. However, this strategy cannot be extended in a natural manner to gas dynamics either with perfect gas law or with real gas state laws.

Therefore, the numerical method we are looking for must have the ability 1) to handle a Euler-type system of equations in regions of high Stokes number or in regions where sub-grid scales induce significant pressure effects, 2) to degenerate to the PGD system in regions of Stokes number below the critical value for particular trajectory crossing or in regions where the subgrid scales do not play any role in particle velocity dispersion, 3) to treat exact vacuum regions for both pressureless and full gas dynamics systems in various regions of the flow. Moreover, this method must feature the same properties of robustness with singularities and vacuum treatment as the Bouchut's kinetic scheme for PGD proposed in de Chaisemartin (2009); Massot et al. (2009). Finally, since the pressure law can bear some real gas effects, the numerical method has to handle such cases while keeping a high level of accuracy as required by the DNS/LES approach.

In that context, the purpose of the present paper is to introduce a novel numerical method based on relaxation schemes which has the ability to match all the previous requirements. Relaxation methods, introduced in Jin and Xin (1995), and further developed in Suliciu (1998) and Coquel and Perthame (1998), have a common basis: they introduce auxiliary variables in the framework of Godunov schemes in order to treat more easily the strong non-linearity due to the treatment of pressure and state law. They avoid to use complex non-linear Riemann solvers or their approximated versions which can have a very high computational cost with non-standard pressure laws. The non-linearity treatment is replaced by a splitting like strategy in the framework of a linear or linearly degenerate version of the transport step, along with a strong relaxation step related to a singular perturbation parameter. A large literature on the subject has shown the impact of such seminal ideas (Chalons and Coquel (2005), Bouchut (2004), Chalons and Coulombel (2008)).

In this contribution, we conduct three new steps : 1) extending the work of Berthon et al. (2006), we propose a scheme for PGD based on successive energy and pressure relaxation which can deal with vacuum, 2) based on this new scheme, we introduce a hybrid numerical method which can treat both regions with and without pressure and still remain accurate and robust, 3) we finally prove the potential of these schemes by comparing them on several tough test-cases to standard approaches in both 1D and 2D configurations. Since relaxation methods are able to treat arbitrary state law, we only provide the schemes in the framework of ideal gas law; besides we focus on the purely convective part of the system of conservation laws and do not treat the potential stress tensors which can be handled by standard schemes. The article is organized as follows. The first section describes how the Eulerian description of turbulent spray dynamics leads to a gas dynamics-type system of conservation equations. The hybrid relaxation scheme is derived in the second section. Finally, results for relevant test-cases, in 1D/2D and pressureless/pressure/hybrid configurations, are presented and discussed.

1 Eulerian modelling of turbulent spray dynamics

Conservation equations on moments of the particle number density function

At the *mesoscopic* level, spray models have a common basis called the *kinetic model* by analogy with kinetic theory of gases. The spray is described as a statistical cloud of point particles experimenting exchanges of mass, momentum and heat with the carrier phase. This kinetic model is described by a Boltzmann type equation (Eq. 1) for the number density function (NDF) f of the spray, where $f(t, \mathbf{x}, \mathbf{u})\mathrm{d}\mathbf{x}\mathrm{d}\mathbf{u}$ denotes the probable number of particles at time t, in a volume of size $\mathrm{d}\mathbf{x}$ around $\mathbf{x}$, with a velocity in a $\mathrm{d}\mathbf{u}$-neighbourhood of $\mathbf{u}$. As mentioned in the introduction, other physical properties like the particle size and temperature can be introduced in the NDF for a finer description of the spray in the framework of the multi-fluid model introduced in Laurent and Massot (2001) and for which references are to be found in de Chaisemartin (2009). For sake of simplicity, constant particle size (monodisperse spray) and temperature are considered here so these variables will not appear in the equations.

The evolution of the spray NDF is given by the Williams transport equation Williams (1958):

$$\partial_t f + \mathbf{u} \cdot \partial_{\mathbf{x}} f + \partial_{\mathbf{u}} \cdot (\mathbf{F} f) = 0, \qquad (1)$$

where $\mathbf{F}$ is the drag force due to the velocity difference with the gaseous phase and given by the Stokes law:

$$\mathbf{F}(t,\mathbf{x},\mathbf{u}) = \frac{\mathbf{U}(t,\mathbf{x}) - \mathbf{u}}{\tau_p} \quad \text{with } \tau_p = \frac{\rho_l d^2}{18\mu_g}, \tag{2}$$

where $\mathbf{U}$ is the gas velocity at the particle location, τ_p is the particle relaxation time, μ_g is the gas viscosity and ρ_l and d are the mass density and diameter of the particle respectively.

The first possibility is to write conservation equations for the zero and first order moments with respect to the velocity variable at a given time t and position $\mathbf{x}$:

$$n(t,\mathbf{x}) = \int f(t,\mathbf{x})\mathrm{d}\mathbf{u}, \tag{3}$$

$$n(t,\mathbf{x})\,\overline{\mathbf{u}}(t,\mathbf{x}) = \int \mathbf{u} f(t,\mathbf{x})\mathrm{d}\mathbf{u}, \tag{4}$$

where n is the particle density and $\overline{\mathbf{u}}$ is the particle mean velocity. At this stage, there are two different ways of deriving the conservation equations for these two moments according to the value of the particle Stokes number St, defined by: $\mathrm{St} = \tau_p/\tau_K$, where τ_K is the Kolmogorov time microscale.

Pressureless gas system

For low Stokes numbers, particles have a low inertia and do not experiment any trajectory crossings. Accordingly, the velocity dispersion around the averaged velocity $\overline{\mathbf{u}}(t,\mathbf{x},S)$ is assumed to be zero in each direction – the spray is called *mono-kinetic* – and the NDF writes:

$$f(t,\mathbf{x},\mathbf{u}) = n(t,\mathbf{x})\delta(\mathbf{u} - \overline{\mathbf{u}}(t,\mathbf{x})). \tag{5}$$

Such an assumption leads to a closed system of conservation equations given by two partial differential equations in the variables $n(t,\mathbf{x})$ and $\overline{\mathbf{u}}(t,\mathbf{x})$ which express the conservation of the number density of droplets and their momentum respectively:

$$\left\{\begin{array}{rl} \partial_t n + \partial_{\mathbf{x}}\cdot(n\overline{\mathbf{u}}) & = 0, \\ \partial_t(n\,\overline{\mathbf{u}}) + \partial_{\mathbf{x}}\cdot(n\,\overline{\mathbf{u}}\otimes\overline{\mathbf{u}}) & = n\overline{\mathbf{F}}, \end{array}\right. \tag{6}$$

where the Stokes drag $\overline{\mathbf{F}}$ is taken at $\mathbf{u} = \overline{\mathbf{u}}$. Equation (6) is similar to the PGD system with an additional velocity relaxation source term.

Gas dynamics system

As pointed out in the introduction, the mono-kinetic assumption is not verified for larger Stokes number, i.e. for particle relaxation times greater than the Kolmogorov time scale, where the effects of particles trajectory crossings yields the need for additional higher order moment modeling. In particular, these crossings are expected to reduce the particle segregation induced by inertia effects. A way to account for the uncorrelated motion of inertial particles is to the used the mesoscopic formalism proposed by Fevrier et al. (2005), starting from the following decomposition: $\mathbf{u} = \overline{\mathbf{u}}(t,\mathbf{x}) + \delta\mathbf{u}$, where $\delta\mathbf{u}$ is called the random uncorrelated component of the particle velocity. System (6), obtained for a mono-kinetic spray, now becomes (see Kaufmann et al. (2008)):

$$\left\{\begin{array}{rcl} \partial_t n + \partial_{\mathbf{x}}\cdot(n\overline{\mathbf{u}}) & = & 0 \\ \partial_t(n\overline{\mathbf{u}}) + \partial_{\mathbf{x}}\cdot(n\overline{\mathbf{u}}\otimes\overline{\mathbf{u}} + \mathcal{P}) & = & n\overline{\mathbf{F}} + \partial_{\mathbf{x}}\delta\tau \\ \partial_t(n\mathcal{E}) + \partial_{\mathbf{x}}\cdot(n\mathcal{E}\,\overline{\mathbf{u}} + \mathcal{P}\,\overline{\mathbf{u}}) & = & n\overline{\mathbf{F}}\cdot\overline{\mathbf{u}} \\ & & -\,2\frac{n}{\tau}\delta\theta \;+\; \text{add. terms} \end{array}\right. \tag{7}$$

where the total energy reads $\mathcal{E} = \overline{\mathbf{u}}\cdot\overline{\mathbf{u}}/2 + \delta\theta$, with $\delta\theta$ the random uncorrelated energy - defined as half the trace of the random uncorrelated stress tensor – and where $\mathcal{P}$ is called the random uncorrelated pressure which is linked to the random uncorrelated energy through the following equation of state:

$$\mathcal{P} = \frac{2}{3} n\,\delta\theta \tag{8}$$

In system (7), $\delta\tau$ is the deviatoric part of the random uncorrelated motion tensor and it can be modeled by a viscosity assumption. These equations correspond to the case where the gas flow is entirely resolved and no modeling of the gas turbulence is used (DNS approach). In the context of statistical (RANS) filtering (Reeks (1992); Zaichik (1999); Massot et al. (2004); de Chaisemartin (2009)) or LES filtering (Moreau et al. (2005); Riber et al. (2005); Pandya and Mashayek (2002); Zaichik et al. (2009)), the pressure law becomes more complicated than the Eq. (8), involving contributions from turbulent or subgrid motion respectively. The modeled scales involve real gas effects through a modification of the state law, as well as source terms of random uncorrelated energy in the rhs of system (7).

The simplified general form of the system of conservation equation finally considered in the following is then system (7) with $\delta\tau = 0$, without the additional terms in the energy equation but with a potential source term, that is $\frac{2n}{\tau}\delta\theta$ is replaced by $\frac{2n}{\tau}(\delta\theta - \varepsilon_t)$, where ε_t is the energy source term due to subgrid turbulence agitation. From a numerical point of view, we thus isolate the difficulties of solving system (7). They requires numerical method for highly compressible flows. The additional source terms and second order derivatives usually do not lead to numerical difficulties and can be treated through operator splitting, whereas the main difficulties arise from the convective first order part involving the

pressure effects. Therefore, in the next subsection, we will focus on the the lhs and forget temporarily the rhs in order to build the numerical schemes. The strategy adopted is to focus on the perfect gas state law in the following, but using relaxation methods, which can be easily extended to any state law with real gas effects usually encountered in LES. Finally, we also need to be able to treat cases where the random uncorrelated energy can be zero and the previous system degenerates toward the PGD.

2 A hybrid relaxation scheme for gas/pressureless gas dynamics problems

Our objective in this section is to describe a global numerical strategy in 1D, able to deal with both gas dynamics and PGD at the same time, and to handle vacuum. It is based on the concept of relaxation approximation for systems of conservation laws. The basic idea is to propose an enlarged system with a stiff relaxation source term, the solutions of which are expected to converge to the solutions of the initial system in the asymptotic limit. In the following, the notations of the previous section are abandoned and replaced by the usual notations for hyperbolic systems of conservation laws.

Towards a unified treatment of gas and pressureless gas dynamics

We first propose to write the pressureless gas system (6) under the equivalent form

$$\begin{cases} \partial_t \rho + \partial_x(\rho u) = 0, \\ \partial_t(\rho u) + \partial_x(\rho u^2 + p) = 0, \end{cases} \tag{9}$$

with $p = 0$. Then, following the general idea of Coquel and Perthame (1998), we propose to approximate the solutions of this system by the ones of the energy relaxation system

$$\begin{cases} \partial_t \rho + \partial_x(\rho u) = 0, \\ \partial_t(\rho u) + \partial_x(\rho u^2 + p) = 0, \\ \partial_t(\rho E) + \partial_x(\rho E u + p u) = -\lambda \rho \varepsilon, \end{cases} \tag{10}$$

where the so-called relaxation internal and total energies are related by

$$E = \varepsilon + \frac{1}{2}u^2.$$

Importantly, the pressure p here no longer equals zero but obeys for instance a perfect gas equation of state

$$\rho\varepsilon = \frac{p}{\gamma - 1}. \tag{11}$$

At least formally, we observe from the last equation in (10) that the relaxation internal energy $\rho\varepsilon$ tends to zero as the relaxation parameter $\lambda > 0$ goes to infinity. By (11), the solutions of the relaxation system (10) are thus expected to provide a good approximation of the solutions of the PGD for large values of λ. Note that if we define the temperature T and the mathematical entropy S according to the second principle of thermodynamics

$$-TdS = d\varepsilon - pd\tau, \quad \tau = 1/\rho,$$

easy calculations lead to the expected entropy inequality

$$\partial_t(\rho S) + \partial_x(\rho S u) = -\lambda\rho\varepsilon \leq 0.$$

It is important to note that the zero internal energy equilibrium manifold, that is also the zero pressure manifold in the limit of infinite λ, is stable in the sense that for initial data with zero pressure, the dynamics naturally remain with zero pressure.

The numerical procedure we are going to propose in order to approximate the solutions of the pressureless gas dynamics system (6) is very classical in the context of relaxation approximations. It is based on an operator splitting for (10) and is made of two steps that we now briefly describe.

First step: We solve the convective part of the model:

$$\begin{cases} \partial_t \rho + \partial_x(\rho u) = 0, \\ \partial_t(\rho u) + \partial_x(\rho u^2 + p) = 0, \\ \partial_t(\rho E) + \partial_x(\rho E u + p u) = 0, \end{cases} \tag{12}$$

which is nothing but the classical gas dynamics system. We will use the condensed form

$$\partial_t \mathcal{U} + \partial_x \mathcal{F}(\mathcal{U}) = 0 \tag{13}$$

for (12) with clear definitions for $\mathcal{U}$ and $\mathcal{F}(\mathcal{U})$.

Second step: In the second step, the contribution of the stiff relaxation source term is accounted for by solving the ODE system

$$\begin{cases} \partial_t \rho = 0 \\ \partial_t(\rho u) = 0 \\ \partial_t(\rho E) = -\lambda\rho\varepsilon \end{cases} \iff \begin{cases} \partial_t \rho = 0 \\ \partial_t(\rho u) = 0 \\ \partial_t \varepsilon = -\lambda\varepsilon \end{cases} \tag{14}$$

in the asymptotic regime $\lambda \to \infty$. This clearly amounts to keep ρ and ρu unchanged and to set $\varepsilon = 0$, that is $\rho E = \frac{1}{2}\rho u^2$ and $p = 0$.

A pressure relaxation model for gas dynamics

In this paragraph, we propose a pressure relaxation system in order to approximate the solutions of the gas dynamics system (12). Motivated by the seminal work of Jin and Xin (1995) and Suliciu (1998), we propose to relax the nonlinearities associated with the pressure law

p only, and to retain the other ones for the sake of accuracy. With this in mind, we introduce the following non linear first order system with singular perturbation:

$$\begin{cases} \partial_t \rho + \partial_x(\rho u) = 0, \\ \partial_t(\rho u) + \partial_x(\rho u^2 + \Pi) = 0, \\ \partial_t(\rho E) + \partial_x(\rho E u + \Pi u) = 0, \\ \partial_t(\rho \Pi) + \partial_x(\rho \Pi u + a^2 u) = \mu\rho(p - \Pi), \end{cases} \tag{15}$$

that we write for shortness

$$\partial_t \mathcal{V} + \partial_x \mathcal{G}(\mathcal{V}) = \mu \mathcal{R}(\mathcal{V}).$$

As μ goes to infinity, we observe at least formally that the relaxation pressure Π tends to p so that the equilibrium system (12) is recovered in this asymptotic regime. The additional equation associated with Π is easily seen to be equivalent to

$$\partial_t \Pi + u\,\partial_x \Pi + \frac{a^2}{\rho}\partial_x u = \mu(p - \Pi).$$

This equation is then very similar to the one associated with the exact pressure p given by

$$\partial_t p + u\,\partial_x p + \rho c^2\,\partial_x u = 0.$$

The choice of the parameter $a > 0$ is crucial for the stability of the relaxation procedure and is determined by the so-called sub-characteristic condition $a > \rho c$ where c denotes the sound speed.

The first-order system extracted from (15) is hyperbolic and admits the following three eigenvalues,

$$\lambda_1 = u - \frac{a}{\rho}, \quad \lambda_2 = u, \quad \lambda_3 = u + \frac{a}{\rho},$$

with second-order multiplicity for λ_2. We note that λ_1 and λ_3 approximate the characteristic speeds $u - c$ and $u + c$ of (12). Importantly, these eigenvalues are now associated with linearly degenerate characteristic fields. This implies that the Riemann problem associated with (15) (with $\mu = 0$) can be explicitly solved, unlike the one associated with (12). Riemann solutions being the key ingredient to devise Godunov-type methods, this mathematical property justifies the introduction of the relaxation model (15).

Here again, the proposed numerical procedure to approximate the solutions of the gas dynamics system (12) is based on an operator splitting for (15) and is made of two steps:
First step: We solve the convective part of the pressure relaxation model taking $\mu = 0$ in (15):

$$\begin{cases} \partial_t \rho + \partial_x(\rho u) = 0, \\ \partial_t(\rho u) + \partial_x(\rho u^2 + \Pi) = 0, \\ \partial_t(\rho E) + \partial_x(\rho E u + \Pi u) = 0, \\ \partial_t(\rho \Pi) + \partial_x(\rho \Pi u + a^2 u) = 0, \end{cases}$$

or equivalently

$$\partial_t \mathcal{V} + \partial_x \mathcal{G}(\mathcal{V}) = 0. \tag{16}$$

In practice, we will use in this step a Godunov method based on the exact Riemann solution of (16).
Second step: We then solve

$$\begin{cases} \partial_t \rho = 0, \\ \partial_t(\rho u) = 0, \\ \partial_t(\rho E) = 0, \\ \partial_t(\rho \Pi) = \mu\rho(p - \Pi), \end{cases}$$

in the asymptotic regime $\mu \to \infty$. The conservative variables ρ, ρu and ρE are thus constant, while Π is set to be equal to p in this step.

For the sake of completeness, we now give the Riemann solution associated with (16). We propose to take a nonconstant in the Riemann solution and we choose to solve

$$\partial_t a + u\,\partial_x a = 0. \tag{17}$$

The diagonal form of (16)-(17) is given by

$$\begin{cases} \partial_t(\Pi + au) + (u + a\tau)\partial_x(\Pi + au) = 0, \\ \partial_t(\Pi - au) + (u - a\tau)\partial_x(\Pi - au) = 0, \\ \partial_t(\Pi + a^2\tau) + u\,\partial_x(\Pi + a^2\tau) = 0, \\ \partial_t(\varepsilon - \frac{\Pi^2}{2a^2}) + u\,\partial_x(\varepsilon - \frac{\Pi^2}{2a^2}) = 0, \\ \partial_t a + u\,\partial_x a = 0. \end{cases}$$

In other words, the quantities $(\Pi \pm au)$, respectively $(\Pi + a^2\tau)$, $(\varepsilon - \frac{\Pi^2}{2a^2})$ and a, are (strong) Riemann invariants for the eigenvalues $u \pm a\tau$, resp. u. The calculations are left to the reader.
Let be given $\mathcal{V}_L = (\mathcal{U}_L, (\rho\Pi)_L)$ and $\mathcal{V}_R = (\mathcal{U}_R, (\rho\Pi)_R)$ two constant states and let a_L and a_R be two values for a. The self-similar Riemann solution $(x,t) \mapsto \mathcal{V}(x/t; \mathcal{V}_L, \mathcal{V}_R; a_L, a_R)$ associated with (16) and initial data

$$\mathcal{V}(x, t = 0) = \begin{cases} \mathcal{V}_L & \text{if} \quad x < 0, \\ \mathcal{V}_R & \text{if} \quad x > 0, \end{cases}$$

is made of four constant states $\mathcal{V}_L$, $\mathcal{V}_L^*$, $\mathcal{V}_R^*$ and $\mathcal{V}_R$, separated by three contact discontinuities associated with $\lambda_k = \lambda_k(\mathcal{V})$, $k = 1, 2, 3$ and propagating with speeds denoted by $\lambda(\mathcal{V}_L, \mathcal{V}_L^*)$, $\lambda(\mathcal{V}_L^*, \mathcal{V}_R^*)$ and $\lambda(\mathcal{V}_R^*, \mathcal{V}_R)$. More precisely, we have

$$\mathcal{V}(\frac{x}{t}; \mathcal{V}_L, \mathcal{V}_R) = \begin{cases} \mathcal{V}_L & \text{if} \ \ \frac{x}{t} < \lambda(\mathcal{V}_L, \mathcal{V}_L^*), \\ \mathcal{V}_L^* & \text{if} \ \ \lambda(\mathcal{V}_L, \mathcal{V}_L^*) < \frac{x}{t} < \lambda(\mathcal{V}_L^*, \mathcal{V}_R^*), \\ \mathcal{V}_R^* & \text{if} \ \ \lambda(\mathcal{V}_L^*, \mathcal{V}_R^*) < \frac{x}{t} < \lambda(\mathcal{V}_R^*, \mathcal{V}_R), \\ \mathcal{V}_R & \text{if} \ \ \lambda(\mathcal{V}_R^*, \mathcal{V}_R) < \frac{x}{t}. \end{cases}$$

The intermediate states $\mathcal{V}_L^*$, $\mathcal{V}_R^*$, as well as the speeds of propagation, are determined using for all $k = 1, 2, 3$

the continuity of the (strong) Riemann invariants for λ_k across the contact discontinuity associated with λ_l, $l \neq k$. We get after easy calculations $\lambda(\mathcal{V}_L, \mathcal{V}_L^*) = \lambda_1(\mathcal{V}_L) = u_L - a_L\tau_L$, $\lambda(\mathcal{V}_L^*, \mathcal{V}_R^*) = u^*$, $\lambda(\mathcal{V}_R^*, \mathcal{V}_R) = \lambda_3(\mathcal{V}_R) = u_R + a_R\tau_R$ and

$$u_L^* = u_R^* = u^* = \frac{a_L u_L + a_R u_R + \Pi_L - \Pi_R}{a_L + a_R},$$

$$\Pi_L^* = \Pi_R^* = \frac{a_R\Pi_L + a_L\Pi_R - a_L a_R(u_R - u_L)}{a_L + a_R},$$

$$\frac{1}{\rho_L^*} = \frac{1}{\rho_L} + \frac{a_R(u_R - u_L) + \Pi_L - \Pi_R}{a_L(a_L + a_R)},$$

$$\frac{1}{\rho_R^*} = \frac{1}{\rho_R} + \frac{a_L(u_R - u_L) + \Pi_R - \Pi_L}{a_R(a_L + a_R)},$$

$$\varepsilon_L^* = \varepsilon_L - \frac{\Pi_L^2}{2a_L^2} + \frac{\Pi^{*2}}{2a_L^2},$$

$$\varepsilon_R^* = \varepsilon_R - \frac{\Pi_R^2}{2a_R^2} + \frac{\Pi^{*2}}{2a_R^2}.$$

At this stage, the initial states $\mathcal{V}_L$ and $\mathcal{V}_R$ and more precisely the free parameters a_L and a_R are implicitly assumed to be such that the waves in the Riemann solutions are ordered as they should, namely

$$\lambda_1(\mathcal{V}_L) = u_L - \frac{a_L}{\rho_L} < u^\star < \lambda_3(\mathcal{V}_R) = u_R + \frac{a_R}{\rho_R}. \quad (18)$$

Following Bouchut (2004), we define $a_L = a_L(\mathcal{V}_L)$ and $a_R = a_R(\mathcal{V}_R)$ as follows:
if $p_R \geq p_L$

$$\frac{a_L}{\rho_L} = \max(c_L, c_{min}) + \alpha(\frac{p_R - p_L}{\rho_R c_R} + u_L - u_R)_+,$$

$$\frac{a_R}{\rho_R} = \max(c_R, c_{min}) + \alpha(\frac{p_L - p_R}{a_L} + u_L - u_R)_+,$$

if $p_R \leq p_L$

$$\frac{a_R}{\rho_R} = \max(c_R, c_{min}) + \alpha(\frac{p_L - p_R}{\rho_L c_L} + u_L - u_R)_+,$$

$$\frac{a_L}{\rho_L} = \max(c_L, c_{min}) + \alpha(\frac{p_R - p_L}{a_R} + u_L - u_R)_+,$$

with $\alpha = (\gamma + 1)/2$, $c_{min} > 0$ and where $p_{L,R} = p_{L,R}(\mathcal{U}_{L,R})$, $c_{L,R} = c_{L,R}(\mathcal{U}_{L,R})$ are the values of the pressures and sound speeds evaluated on $\mathcal{U}_L$ and $\mathcal{U}_R$.
This choice has several advantages. First, it is shown to fullfil (18) and to give the positivy of the intermediate densities ρ_L^* and ρ_R^*. Then, it complies with the subcharacteristic condition $a > \rho c$. At last, it guarantees the nonlinear stability of the underlying relaxation scheme that will be described in the next paragraph, and the possibility of handling vacuum in the sense that the speeds of propagation $\lambda_1(\mathcal{V}_L)$ and $\lambda_3(\mathcal{V}_R)$ remain finite. In particular, discrete entropy inequalities as well as maximum principles can be proved. These results are pretty technical to establish and are not presented in this paper. We refer the reader to Bouchut (2004) for the details.
In the case of PGD, these formulas are to be considered with $p_L = p_R = 0$ and $c_L = c_R = 0$. We then observe that the threshold c_{min} allows to guarantee (18) when $u_L \leq u_R$ and then to avoid the resonance phenomenon.

A relaxation scheme for the gas and pressureless gas dynamics

In this paragraph, we present a relaxation scheme for approximating the solutions of the gas or pressureless gas dynamics equations (13) and (10) separately. The case of mixed computations involving both the gas and pressureless gas dynamics at the same time will be considered in the next paragraph. It is important to notice that the same formalism will be used for both systems. Just note that in the pressureless case, E must be understood as a function of the unknowns ρ and ρu, namely

$$E = \frac{(\rho u)^2}{2\rho},$$

but not as an unknown with evolution given by the passive transport equation

$$\partial_t \rho E + \partial_x(\rho E u) = 0.$$

Initial condition is denoted

$$\mathcal{U}(x, 0) = \mathcal{U}_0(x),$$

with $E_0(x) = \frac{(\rho u)_0^2(x)}{2\rho_0(x)}$ in the case of PGD.
We first set some notations. Let Δx and Δt be two constant steps for space and time discretizations. Let $(x_j)_{j\in\mathbb{Z}}$ be a sequence of equidistributed points in $\mathbb{R}$: $x_{j+1} - x_j = \Delta x$. For all $j \in \mathbb{Z}$ and all $n \in \mathbb{N}$, we define

$$x_{j+1/2} = x_j + \frac{\Delta x}{2}, \quad t^n = n\Delta t,$$

and consider the following discretization of the computational domain $\mathbb{R}_x \times \mathbb{R}_t^+$:

$$\mathbb{R}_x \times \mathbb{R}_t^+ = \bigcup_{j\in\mathbb{Z}} \bigcup_{n\geq 0} C_j^n,$$

with

$$C_j^n = [x_{j-1/2}, x_{j+1/2}[\times[t^n, t^{n+1}[.$$

On the one hand and as usual in the context of finite volume methods, the approximate solution $\mathcal{U}_{\Delta t,\Delta x}(x, t)$ of

(13) or (10) with initial data $\mathcal{U}_0$ is sought as a piecewise constant function on each slab C_j^n:

$$\mathcal{U}_{\Delta t,\Delta x}(x,t) = \mathcal{U}_j^n \text{ for } (x,t) \in C_j^n.$$

At time $t = 0$, we set

$$\mathcal{U}_j^0 = \frac{1}{\Delta x}\int_{x_{j-1/2}}^{x_{j+1/2}} \mathcal{U}_0(x)dx, \quad j \in \mathbb{Z}.$$

On the other hand, we define from $\mathcal{U}_{\Delta t,\Delta x}$ the piecewise constant approximate solution $\mathcal{V}_{\Delta t,\Delta x}$ by

$$\mathcal{V}_{\Delta t,\Delta x}(x,t) = \mathcal{V}_j^n = \begin{pmatrix} \mathcal{U}_j^n \\ (\rho\Pi)_j^n \end{pmatrix} \text{ for } (x,t) \in C_j^n.$$

This solution is set to be at *equilibrium*, that is

$$(\rho\Pi)_j^n = p(\mathcal{U}_j^n), \quad j \in \mathbb{Z}$$

for the gas dynamics and

$$(\rho\Pi)_j^n = 0, \quad j \in \mathbb{Z}$$

for the PGD.
Let us assume that the solution $\mathcal{U}_{\Delta t,\Delta x}(x,t^n)$ at time t^n is known. In order to advance it to the next time level t^{n+1}, we now describe the two steps of the method in details.

First step: evolution in time $(t^n \to t^{n+1-})$
In this step, we solve (16) with $\mathcal{V}_{\Delta t,\Delta x}(x,t^n)$ as initial data and for times $t \in [0,\Delta t]$. Under the CFL condition

$$\frac{\Delta t}{\Delta x}\max_{\mathcal{V}}(|\lambda_i(\mathcal{V})|, i = 1,2,3) < \frac{1}{2} \tag{19}$$

where the maximum is taken over all the $\mathcal{V}$ under consideration, the solution is obtained by solving a sequence of non interacting Riemann problems set at each cell interface $x_{j+1/2}$. It is explicitly known by the previous paragraph and we have

$$\mathcal{V}(x,t) = \mathcal{V}(\tfrac{x-x_{j+1/2}}{t}; \mathcal{V}_j^n, \mathcal{V}_{j+1}^n; a_L(\mathcal{V}_j^n), a_R(\mathcal{V}_{j+1}^n)),$$
$$\text{for } (x,t) \in [x_j, x_{j+1}]\times]0,\Delta t], \quad j \in \mathbb{Z}.$$

We then get back a piecewise constant function in $x \in [x_{j-1/2}, x_{j+1/2}]$ by means of a classical L^2 projection, that is

$$\tilde{\mathcal{V}}(x,t) = \frac{1}{\Delta x}\int_{x_{j-1/2}}^{x_{j+1/2}} \mathcal{V}(x,t)dx,$$
$$\text{for } (x,t) \in [x_{j-1/2}, x_{j+1/2}]\times]0,\Delta t], \ j \in \mathbb{Z},$$

and we set

$$\mathcal{V}_j^{n+1-} = \begin{pmatrix} \mathcal{U}_j^{n+1-} \\ (\rho\Pi)_j^{n+1-} \end{pmatrix} = \tilde{\mathcal{V}}(x_j,\Delta t), \quad j \in \mathbb{Z}. \tag{20}$$

Of course, this first step is nothing but the celebrated Godunov method applied to (16). As a consequence, the update formula (20) can easily be given the following conservation form

$$\mathcal{V}_j^{n+1-} = \mathcal{V}_j^n - \frac{\Delta t}{\Delta x}(g(\mathcal{V}_j^n, \mathcal{V}_{j+1}^n) - g(\mathcal{V}_{j-1}^n, \mathcal{V}_j^n)),$$
$$j \in \mathbb{Z}, \quad n \geq 0,$$

where the numerical flux function writes for all $j \in \mathbb{Z}$

$$g(\mathcal{V}_j^n, \mathcal{V}_{j+1}^n) = \mathcal{G}\Big(\mathcal{V}\big(0; \mathcal{V}_j^n, \mathcal{V}_{j+1}^n; a_L(\mathcal{V}_j^n), a_R(\mathcal{V}_{j+1}^n)\big)\Big). \tag{21}$$

Let us recall that the numerical flux (21) is here explicitly known.

Second step: relaxation $(t^{n+1-} \to t^{n+1})$
We now project the solution $\mathcal{V}_{\Delta t,\Delta x}(x,t^{n+1-})$ obtained at the end of the previous step on the equilibrium manifold $\mu = +\infty$. More precisely, we set for all $j \in \mathbb{Z}$

$$\mathcal{V}_j^{n+1} = \begin{pmatrix} \mathcal{U}_j^{n+1} \\ (\rho\Pi)_j^{n+1} \end{pmatrix} \tag{22}$$

with

$$\mathcal{U}_j^{n+1} = \mathcal{U}_j^{n+1-} \quad \text{and} \quad (\rho\Pi)_j^{n+1} = p(\mathcal{U}_j^{n+1})$$

in the case of the gas dynamics equations, and

$$\mathcal{U}_j^{n+1} = (\rho, \rho u, \frac{(\rho u)^2}{2\rho})_j^{n+1-} \quad \text{and} \quad (\rho\Pi)_j^{n+1} = 0$$

in the pressureless case. This is equivalent to solve in the asymptotic regime $\mu = +\infty$

$$\begin{cases} \partial_t\rho = 0, \\ \partial_t(\rho u) = 0, \\ \partial_t(\rho E) = 0, \\ \partial_t(\rho\Pi) = -\mu\rho(p - \Pi), \end{cases} \tag{23}$$

in the case of the gas dynamics equations, and

$$\begin{cases} \partial_t\rho = 0, \\ \partial_t(\rho u) = 0, \\ \partial_t(\rho E) = -\lambda\rho\varepsilon, \\ \partial_t(\rho\Pi) = -\mu\rho(p - \Pi), \end{cases} \tag{24}$$

in the case of PGD.

In agreement with the description of these two steps, the approximate solution $\mathcal{U}_{\Delta t,\Delta x}$ is then updated according to the following consistent finite volume method:

$$\begin{aligned} \rho_j^{n+1} &= \rho_j^n - \frac{\Delta t}{\Delta x}\Delta f^\rho(\mathcal{U}_j^n, \mathcal{U}_{j+1}^n), \\ (\rho u)_j^{n+1} &= (\rho u)_j^n - \frac{\Delta t}{\Delta x}\Delta f^{\rho u}(\mathcal{U}_j^n, \mathcal{U}_{j+1}^n), \end{aligned} \tag{25}$$

together with

$$(\rho E)_j^{n+1} = (\rho E)_j^n - \frac{\Delta t}{\Delta x}\Delta f^{\rho E}(\mathcal{U}_j^n, \mathcal{U}_{j+1}^n) \quad (26)$$

in the case of gas dynamics and

$$(\rho E)_j^{n+1} = (\frac{(\rho u)^2}{2\rho})_j^{n+1} \quad (27)$$

in the case of PGD. Here of course, $(f^\rho, f^{\rho u}, f^{\rho E})(\mathcal{U}_j^n, \mathcal{U}_{j+1}^n)$ denote the first three components of $g(\mathcal{V}_j^n, \mathcal{V}_{j+1}^n)$ and

$$\Delta f^\alpha(\mathcal{U}_j^n, \mathcal{U}_{j+1}^n) = f^\alpha(\mathcal{U}_j^n, \mathcal{U}_{j+1}^n) - f^\alpha(\mathcal{U}_{j-1}^n, \mathcal{U}_j^n)$$

for $\alpha = \rho, \rho u, \rho E$.

Coupling the gas and pressureless gas dynamics

In order to perform computations involving both the gas and PGD at the same time, we have to describe how to couple the relaxation schemes we have developed for both systems. Recall that the conservative unknowns are ρ, ρu and ρE for the gas dynamics and ρ and ρu for the PGD. The main difference then clearly lies in the treatment of the energy equation.

For the sake of clarity, we begin by introducing a color function Y such that $Y = 1$ for gas dynamics and $Y = 0$ for PGD. From a numerical point of view, a given cell $\mathcal{C}_j^n$ is said to be *pressureless*, or equivalently such that $Y_j^n = 0$, if the internal energy $\varepsilon_j^n = (\rho E - \frac{(\rho u)^2}{2\rho})_j^n$ is less than a given threshold ε_{min} and *with pressure*, that is $Y_j^n = 1$, otherwise. Introducing the threshold ε_{min} is a convenient way to switch from one algorithm to the other. In agreement with the threshold c_{min} already introduced for the sound speed in the definition of a_L and a_R, we set

$$\varepsilon_{min} = \frac{c_{min}^2}{\gamma(\gamma - 1)}. \quad (28)$$

Recall indeed that for perfect gas equations of state we have $c^2 = \gamma(\gamma-1)\varepsilon$. We thus distinguish between zones with PGD where the internal energy is exactly zero and zones where the energy level is above the defined small threshold, a property which is preserved by the pure convective part of the evolution.

Let us consider a given cell $\mathcal{C}_j^n$. Four different situations must be distinguished, depending in particular on whether $Y_{j-1}^n = Y_j^n = Y_{j+1}^n$ or not.

The case $Y_{j-1}^n = Y_j^n = Y_{j+1}^n = 0$. In this case, we simply use (25) and (27) without any modification.

The case $Y_{j-1}^n = Y_j^n = Y_{j+1}^n = 1$. In this case, we simply use (25) and (26) without any modification.

The case $Y_{j-1}^n \neq Y_j^n$ *and/or* $Y_{j+1}^n \neq Y_j^n$. In this case, we consider that the cell $\mathcal{C}_j^n$ should be considered *with pressure* in the update formula. Thus, we propose to use

$$\begin{aligned} \rho_j^{n+1} &= \rho_j^n - \frac{\Delta t}{\Delta x}\Delta f^\rho(\overline{\mathcal{U}}_j^n, \overline{\mathcal{U}}_{j+1}^n), \\ (\rho u)_j^{n+1} &= (\rho u)_j^n - \frac{\Delta t}{\Delta x}\Delta f^{\rho u}(\overline{\mathcal{U}}_j^n, \overline{\mathcal{U}}_{j+1}^n), \end{aligned} \quad (29)$$

and

$$(\rho E)_j^{n+1} = \overline{(\rho E)}_j^n - \frac{\Delta t}{\Delta x}\Delta f^{\rho E}(\overline{\mathcal{U}}_j^n, \overline{\mathcal{U}}_{j+1}^n) \quad (30)$$

where for $k = j-1, j, j+1$, $\overline{\mathcal{U}}_k^n = \mathcal{U}_k^n$ if $Y_k^n = 1$ and

$$\overline{\mathcal{U}}_k^n = (\rho, \rho u, \overline{\rho E})_k^n, \quad \overline{\rho E}_k^n = \rho_k^n \varepsilon_{min} + (\frac{(\rho u)^2}{2\rho})_k^n$$

otherwise.

Extension to $2D$ configurations and to second-order accuracy

So far, we focused ourselves on the mono-dimensional case. In order to perform the $2D$ computations presented in the next section on cartesian meshes, we used a very classical dimensional splitting method. We briefly recall that it first consists in splitting the two-dimensional governing equations into a pair of quasi one-dimensional equations, and then to solve the underlying sequence of two one-dimensional problems with the proposed numerical strategy. Recall that if we denote (u, v) the two components of the velocity field, v being associated with the additional space dimension, the governing equation for v in the quasi-$1D$ system reads

$$\partial_t(\rho v) + \partial_x(\rho v u) = 0. \quad (31)$$

This equation means that v is simply passively transported with the flow. From a numerical point of view, a natural discretisation of (31) is given by

$$(\rho v)_j^{n+1} = (\rho v)_j^n - \frac{\Delta t}{\Delta x}\Delta f^{\rho v}(\mathcal{U}_j^n, \mathcal{U}_{j+1}^n),$$

with

$$\Delta f^{\rho v}(\mathcal{U}_j^n, \mathcal{U}_{j+1}^n) = f^{\rho v}(\mathcal{U}_j^n, \mathcal{U}_{j+1}^n) - f^{\rho v}(\mathcal{U}_{j-1}^n, \mathcal{U}_j^n)$$

and

$$f^{\rho v}(\mathcal{U}_j^n, \mathcal{U}_{j+1}^n) = \begin{cases} f^\rho(\mathcal{U}_j^n, \mathcal{U}_{j+1}^n)\ v_j^n & \text{if} \quad f^\rho(\mathcal{U}_j^n, \mathcal{U}_{j+1}^n) \geq 0, \\ f^\rho(\mathcal{U}_j^n, \mathcal{U}_{j+1}^n)\ v_{j+1}^n & \text{if} \quad f^\rho(\mathcal{U}_j^n, \mathcal{U}_{j+1}^n) \leq 0. \end{cases}$$

This formula has been first introduced in Larrouturou (1991) and complies with the exact resolution of the Riemann problem for the quasi-$1D$ relaxation model

$$\begin{cases} \partial_t \rho + \partial_x(\rho u) = 0, \\ \partial_t(\rho u) + \partial_x(\rho u^2 + \Pi) = 0, \\ \partial_t(\rho E) + \partial_x(\rho E u + \Pi u) = 0, \\ \partial_t(\rho \Pi) + \partial_x(\rho \Pi u + a^2 u) = 0, \\ \partial_t(\rho v) + \partial_x(\rho v u) = 0. \end{cases}$$

The calculations are left to the reader. The second-order extension in space we used in the numerical experiments is based on a very classical MUSCL reconstruction technique on the primitive variables ρ, u and ε, using a min-mod slope limiter. Regarding the time second-order extension, we used an usual Runge-Kutta method coupled with a Strang splitting.

3 Results and discussion

1D Bouchut test

To evaluate the performance of the present relaxation scheme in the PGD configuration, the first numerical test of Bouchut et al. (2003) is performed. In this test, the initial solution is designed to create a vacuum state and a mass accumulation. Figure 1 compares the results between Bouchut's kinetic scheme and the relaxation scheme for first and second orders. Figure 1.a shows that vacuum is properly captured by the first and second order relaxation schemes. As noticed by Bouchut et al. (2003), the first order scheme forms an artificial density peak. This problem does not appear for both second order schemes. Compared to Bouchut's scheme, the second order relaxation scheme is slightly more diffusive and the density overshoots created in the zone of negative velocity divergence are a little bit stronger. All the schemes capture perfectly the discontinuity of the velocity in the vacuum region (see Fig. 1.b). In the mass accumulation zone, the most accurate results are obtained with Bouchut's scheme which is closely followed by the second order relaxation scheme.

1D Sod shock tube

In order to evaluate the hybrid PGD/gas dynamics relaxation method, the Sod shock tube test is performed with the following initial conditions:

$$v^0 = 0, \quad \begin{cases} \rho^0 & = 1, \quad p^0 = 1.1 \quad \text{if} \quad x \leq 0.5 \\ \rho^0 & = 0.125, \quad p^0 = 0 \quad \text{if} \quad x > 0.5 \end{cases}$$

At the initial time, $x > 0$ corresponds to a zero pressure field computed with the pressureless gas algorithm while $x \leq 0$ is computed with the gas dynamics algorithm. In this test case as in all other coupled method calculations, $c_{min} = 10^{-5}$ and ε is evaluated through Eq. (28). Figures 2 shows the density and pressure profiles at time $t = 0.1644$ for the first and second order relaxation schemes. The interface between pressure and pressureless regions does not present any numerical artefact. Due to the poor discretization of the surface discontinuity and the shock, the density solution is smeared by the numerical diffusion. The second order scheme presents a significantly better accuracy than the first order one.

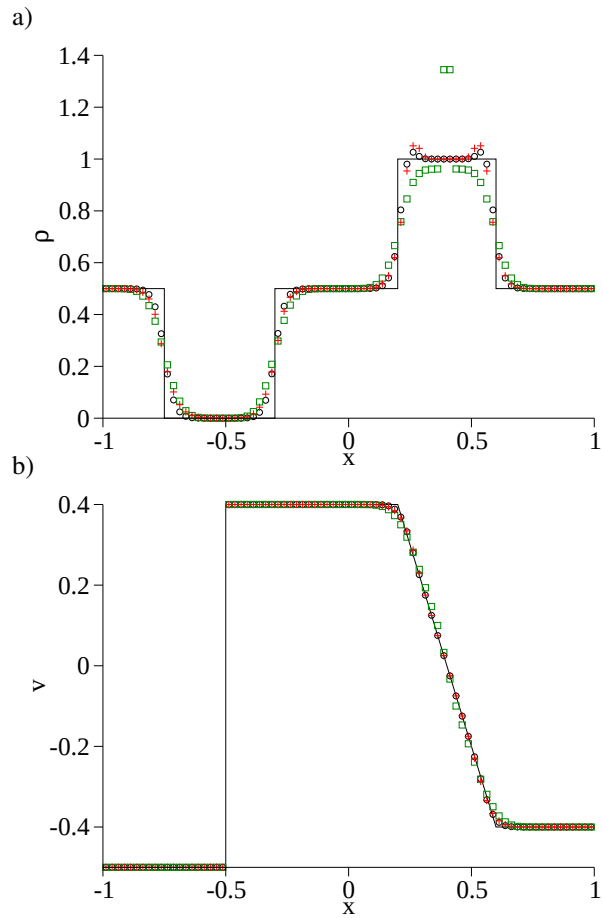

Figure 1: Profiles of density (a) and velocity (b) for Bouchut numerical test at time $t=0.5$: exact solution (—), 2nd order Bouchut scheme (○), 1^{rst} order relaxation scheme (□), 2nd order relaxation scheme (+) (80 nodes, CFL$=0.5$).

1D Shock/δ-shock interaction

The robustness of the second-order relaxation scheme is tested in a configuration where a shock propagates through a pressureless region and meets a δ-shock in density. The δ-shock is created by an initial velocity perturbation located in the pressureless region (see black line in Fig. 3.b). Figure 3 shows two instants of the calculation: before $(t = 0.1)$ and after $(t = 0.5)$ the shock meets the δ-shock. The trace of this interaction on the velocity profile is an n-wave downstream the shock position (Fig. 3.b). A corresponding density n-wave appears on Fig. 3.a. After having interacted with the δ-shock $(t = 0.5)$, the shock has a higher density ratio than before $(t = 0.1)$ whereas its velocity jump stays unchanged. This test demonstrates the high robustness of the present relaxation scheme.

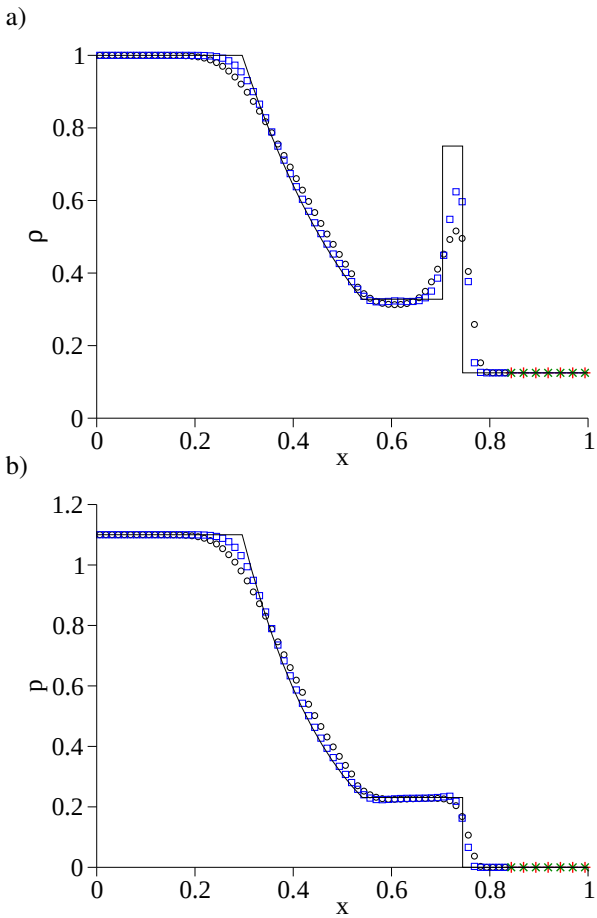

Figure 2: Profiles of density (a) and pressure (b) for the hybrid relaxation scheme in Sod numerical test at time $t = 0.1644$: 1^{rst} order relaxation scheme (pressure region: $\circ$, pressureless region: $+$), 2nd order relaxation scheme (pressure region: $\square$, pressureless region: $\times$) (80 nodes, CFL $= 0.5$).

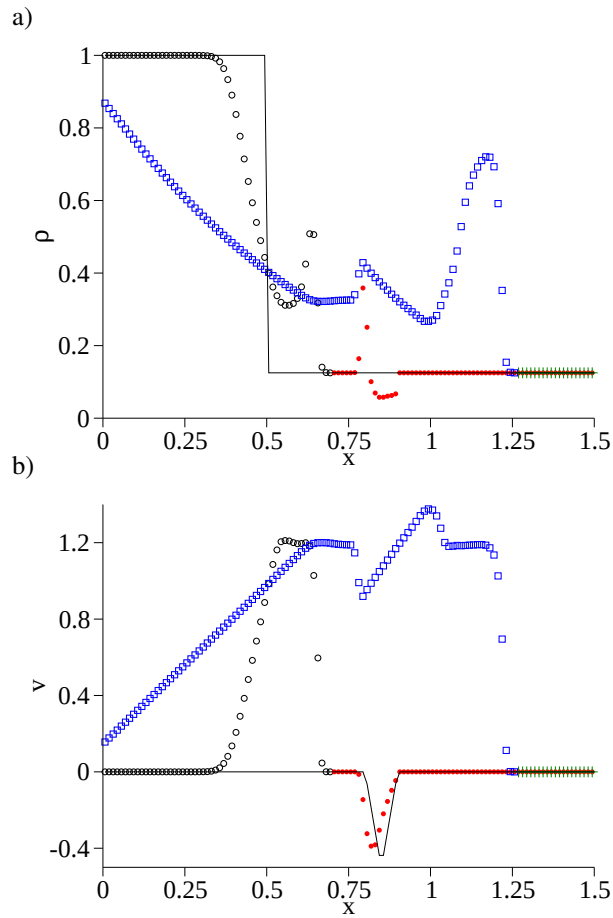

Figure 3: Second order hybrid relaxation scheme calculation of the interaction of a shock/δ-shock: profiles of density (a) and velocity (b) at time $t = 0$ (—), $t = 0.1$ (before the interaction, pressure region: $\circ$, pressureless region: $\bullet$) and $t = 0.5$ (after the interaction, pressure region: $\square$, pressureless region: $+$) (120 nodes, CFL $= 0.5$).

2D Taylor-Green vortices

Figure 4.a shows the velocity field $\mathbf{U} = (U, V)$ of the carrier phase corresponding to the four contra-rotating Taylor-Green vortices used in the following numerical tests:

$$\begin{cases} U(x,y) &= \sin(2\pi x)\cos(2\pi y) \\ V(x,y) &= -\cos(2\pi x)\sin(2\pi y) \end{cases}$$

The spray dynamics is coupled to the gaseous flow field through a Stokes drag source term in the momentum equation, which amounts to relaxing the spray velocity field toward the gaseous one at a rate set by the Stokes number St, i.e. the non dimensional relaxation time. From de Chaisemartin (2009) we know that there exists a critical value $\mathrm{St}_c = 1/8\pi$ which separates two regimes. For $\mathrm{St} < \mathrm{St}_c$, the particles cannot escape from the Taylor-Green vortices while, for $\mathrm{St} \geq \mathrm{St}_c$, they are ejected out of their original vortices. Therefore, the following tests consider two values of St in order to cover these two regimes: $\mathrm{St} = 0.9\mathrm{St}_c$ and $\mathrm{St} = 13\mathrm{St}_c$. From a numerical point of view, the drag source term $\overline{\mathbf{F}}$ is applied via operator splitting through an analytical expression of the exponential relaxation (Eq. 10). The initial spray velocity is uniformly zero for all test-cases.

Pressureless transport of a non-uniform initial distribution at supercritical Stokes number. In order to test the capability of the method to treat multidimensional transport of inertial particles, the Stokes number is fixed at a supercritical value $\mathrm{St} = 13\mathrm{St}_c$. Figure 4.a

shows the initial density distribution provided by a cardinal sinus function. To allow comparison with Bouchut's scheme, the pressureless relaxation scheme is used. Figure 4.b and 4.c show the results at time $t = 0.8$ for the second order Bouchut scheme and the second order relaxation scheme. Both schemes predict very similar density fields featuring a δ-shock, as expected (see de Chaisemartin (2009)).

Pressure vs pressureless transport of an uniform initial distribution at subcritical Stokes number. Figures 5.a and 5.b compares the density fields obtained with the second order Bouchut scheme and the second order relaxation scheme respectively, starting from a uniform density distribution in subcritical Stokes number conditions $\mathrm{St} = 0.9\mathrm{St}_c$. As for the supercritical case, both schemes predict very similar results, with mass concentrating in the high strain regions because of the ejection of particles from the center of vortices. The hybrid second order scheme still being under development, calculations of the standard gas dynamics relaxation scheme are presented only for the first order scheme. In order to limit the effect of different numerical diffusion according to the scheme order, a spatial resolution of two times larger is used for the gas dynamics first order scheme (400 nodes vs. 200 nodes for the second order calculations). Figure 5.c shows that pressure effects limits the segregation of particles (density concentration here). Physically, this can be interpreted as a mixing effect from the carrier flow turbulence. Here, this turbulence is very simply modeled by a uniform relaxation term of internal energy (target value $\varepsilon_t = 1$).

Hybrid pressure/pressureless transport of a non-uniform initial distribution at supercritical Stokes number. The hybrid scheme is evaluated in a configuration where two parcels of high-inertia particles are ejected from their initial vortices and collide together. The density distribution is given by a cardinal sinus function whose center is $(0.125, \pm 0.375)$ and radius 0.125 (see Fig. 6). A PGD calculation and a gas dynamics calculation are performed. For the gas dynamics case, a relaxation term of internal energy is imposed using a cardinal sinus function centered on $y = 0$ with a radius of 0.125 and a maximum value of $\varepsilon_t = 0.5$ (see Fig. 6.b). This energy source term simulates the effect of a local turbulence region of the carrier flow on the particles transport. As expected, Fig. 6 shows that, for both PGD and hybrid schemes, each particle parcel is ejected from its vortex and start to interact with its mirror image at $t = 0.75$. In the PGD case (Fig. 6.a), this interaction forms a δ-shock at the meeting line $y = 0$. On the other hand, the hybrid case (Fig. 6.b) features only a small increase in density at $y = 0$ because pressure effects limit the concentration of particles. Later, the behavior of both schemes are even more different (see Fig. 6.c and d). Most of the density is concentrated close to $y = 0$ in the PGD case, while a smoother density distribution is observed in the hybrid case. Note that with the hybrid scheme, the maximum of density is not located on the $y = 0$ line because the pressure gradient resulting from the energy source term prevents particles from accumulating there.

Conclusions

A novel hybrid numerical method for solving Eulerian models for spray dynamics has been proposed. Based on the relaxation method, it can deal with both PGD and general gas dynamics system of equations in various zones of the same configuration. Therefore, it has the ability, on the one hand, to compute the low-inertia particles dynamics – described by PGD – and, on the other hand, to account for the effects of high-inertia particles in the turbulent regions of the flow — falling under the general gas dynamics framework. The zero-density is also explicitely handled, which is a key feature for simulating spray injection. In terms of accuracy, one and two-dimensional tests in PGD configurations show that the scheme matches the kinetic scheme of Bouchut previously used and thus validate the approach. Beside, the hybrid PGD/gas dynamics approach predicts accurate results in the 1D shock tube test-case. The high robustness of the method is demonstrated, in particular in a shock/δ-shock interaction. Two-dimensional simulations in the framework of Taylor-Green vortices with eventually localized turbulent subgrid energy source allow to exhibit the potential of the method. Besides, the relaxation framework makes it possible to handle arbitrary pressure law such as the real gas-type behaviour of turbulent sprays. Therefore the present investigation shows that this method has the ingredients needed to simulate turbulent sprays in a DNS/LES framework.

Acknowledgements

Quang Huy Tran from IFP is gratefully acknowledged for his precious help to the present work.

References

C. Berthon, M. Breuß, and M.O. Titeux. A relaxation scheme for the approximation of the pressureless Euler equations. *Numer. Methods for Partial Differential Equations*, 22(2):484–505, 2006.

G. A. Bird. *Molecular gas dynamics and the direct simulation of gas flows*, volume 42 of *Oxford Engineering Science Series*. Oxford University Press, 1994.

M. Boileau, S. Pascaud, E. Riber, B. Cuenot, L.Y.M. Gicquel, T. Poinsot, and M. Cazalens. Investigation of two-fluid methods for Large Eddy Simulation of spray combustion in Gas Turbines. *Flow Turbul. Combust.*, 80 (3):291–321, 2008a.

M. Boileau, G. Staffelbach, B. Cuenot, T. Poinsot, and C. Bérat. LES of an ignition sequence in a gas turbine engine. *Combust. Flame*, 154(1–2):2–22, 2008b.

F. Bouchut. *Nonlinear stability of finite volume methods for hyperbolic conservation laws, and well-balanced schemes for sources*. Frontiers in Mathematics. Birkhäuser Verlag, Basel, 2004.

F. Bouchut, S. Jin, and X. Li. Numerical approximations of pressureless and isothermal gas dynamics. *SIAM J. Numer. Anal.*, 41(1):135–158, 2003.

C. Chalons and F. Coquel. Navier-stokes equations with several independent pressure laws and explicit predictor-corrector schemes. *Numer. Math.*, 101(3):451–478, 2005.

C. Chalons and J.-F. Coulombel. Relaxation approximation of the euler equations. *J. Math. Anal. Appl.*, 348(2): 872–893, 2008.

F. Coquel and B. Perthame. Relaxation of energy and approximate riemann solvers for general pressure laws in fluid dynamics. *SIAM J. Numer. Anal.*, 35(6):2223–2249, 1998.

S. de Chaisemartin. *Modèles eulériens et simulation numérique de la dispersion turbulente de brouillards qui s'évaporent*. PhD thesis, Ecole Centrale Paris, http://tel.archives-ouvertes.fr/tel-00443982/en/, 2009.

F. Duchaine, T. Morel, and L.Y.M. Gicquel. Computational-Fluid-Dynamics-Based Kriging Optimization Tool for Aeronautical Combustion Chambers. *AIAA J.*, 47(3), 2009.

P. Fevrier, O. Simonin, and K. Squires. Partitioning of particle velocities in gas-solid turbulent flows into a continuous field and a spatially uncorrelated random distribution theoretical formalism and numerical study. *J.Fluid Mech*, 533:1–46, 2005.

L. Fréret, S. de Chaisemartin, J. Reveillon, F. Laurent, and M. Massot. Eulerian models and three-dimensional numerical simulation of polydisperse sprays. In *Proc. 7th Int. Conf. Multiphase Flow, Tampa, FL, USA*, 2010.

M. Garcia. *Development and validation of the Euler-Lagrange formulation on a parallel and unstructured solver for large-eddy simulation*. PhD thesis, Institut National Polytechnique de Toulouse, http://tel.archives-ouvertes.fr/tel-00414067/en/, 2009.

J. B. Greenberg, I. Silverman, and Y. Tambour. On the origin of spray sectional conservation equations. *Combust. Flame*, 93:90–96, 1993.

S. Jin and Z. Xin. The relaxation schemes for systems of conservation laws in arbitrary space dimensions. *Comm. Pure Appl. Math.*, 48(3), 1995.

D. Kah, F. Laurent, L. Fréret, S. de Chaisemartin, R.O. Fox, J. Reveillon, and M. Massot. Eulerian quadrature-based moment models for dilute polydisperse evaporating sprays. *Flow Turbul. Combust.*, http://hal.archives-ouvertes.fr/hal-00449866/en/ 2010.

A. Kaufmann, M. Moreau, O. Simonin, and J. Helie. Comparison between Lagrangian and mesoscopic Eulerian modelling approaches for inertial particles suspended in decaying isotropic turbulence. *J. Comput. Phys.*, 227(13):6448 – 6472, 2008.

G. Lacaze, B. Cuenot, T. Poinsot, and M. Oschwald. Large eddy simulation of laser ignition and compressible reacting flow in a rocket-like configuration. *Combust. Flame*, 156(6):1166–1180, 2009.

B. Larrouturou. How to preserve the mass fractions positivity when computing compressible multi-component flows. *J. Comput. Phys.*, 95:59–84, 1991.

F. Laurent and M. Massot. Multi-fluid modeling of laminar poly-dispersed spray flames: origin, assumptions and comparison of sectional and sampling methods. *Comb. Theory and Modelling*, 5:537–572, 2001.

M. Massot. Eulerian multi-fluid models for polydisperse evaporating sprays. In *Multiphase reacting flows: modelling and simulation*, volume 492 of *CISM Courses and Lectures*, pages 79–123. Springer, 2007. Editors D.L. Marchisio and R. O. Fox, Udine, July 2006.

M. Massot, R. Knikker, C. Péra, and J. Reveillon. Lagrangian/Eulerian analysis of the dispersion of evaporating sprays in non-homogeneous turbulent flows. In *Proc. 5th Int. Conf. Multiphase Flow*, 2004.

M. Massot, F. Laurent, S. de Chaisemartin, L. Fréret, and D. Kah. Eulerian multi-fluid models: modeling and numerical methods. In *Modelling and Computation of Nanoparticles in Fluid Flows*, Lecture Notes of the von Karman Institute. NATO RTO AVT-169, 2009. In Press http://hal.archives-ouvertes.fr/hal-00423031/en/.

M. Moreau, B. Bédat, and O. Simonin. A priori testing of subgrid stress models for euler-euler two-phase LES from euler-lagrange simulations of gas-particle turbulent flow. In *18th Ann. Conf. on Liquid Atomization and Spray Systems*. ILASS Americas, 2005.

P. J. O'Rourke. *Collective drop effects on vaporizing liquid sprays*. PhD thesis, Princeton University, 1981.

R.V.R. Pandya and F. Mashayek. Two-fluid large-eddy simulation approach for particle-laden turbulent flows. *Int. J. Heat Mass Transfer*, 45(24):4753–4759, 2002.

M.W. Reeks. On the continuum equations for dispersed particles in nonuniform flows. *Phys. Fluids A*, 4(6): 1290–1303, 1992.

E. Riber, M. Moreau, O. Simonin, and B. Cuenot. Towards large eddy simulation of non-homogeneous particle laden turbulent gas flows using euler-euler approach. In *11th Workshop on Two-Phase Flow Predictions, Merseburg, Germany*, 2005.

E. Riber, V. Moureau, M. García, T. Poinsot, and O. Simonin. Evaluation of numerical strategies for large eddy simulation of particulate two-phase recirculating flows. *J. Comput. Phys.*, 228(2):539–564, 2009.

A. Roux, L.Y.M. Gicquel, Y. Sommerer, and T. Poinsot. Large eddy simulation of mean and oscillating flow in side-dump ramjet combustor. *Combust. Flame*, 152(1-2):154–176, 2008.

L. Selle, L. Benoit, T. Poinsot, F. Nicoud, and W. Krebs. Joint use of compressible large-eddy simulation and helmholtz solvers for the analysis of rotating modes in an industrial swirled burner. *Combust. Flame*, 145(1-2): 194–205, 2006.

O. Simonin, P. Février, and J. Laviéville. On the spatial distribution of heavy-particle velocities in turbulent flow: from continuous field to particulate chaos. *J. Turbul.*, 3(40):1–18, 2002.

I. Suliciu. Energy estimates in rate-type thermoviscoplasticity. *Int. J. Plast.*, 14:227–244, 1998.

A. Vié, M. Sanjosé, S. Jay, C. Angelberger, B. Cuenot, and M. Massot. Evaluation of a multifluid mesoscopic eulerian formalism on the Large Eddy Simulation of an aeronautical-type configuration. In *Proc. 7th Int. Conf. Multiphase Flow, Tampa, FL, USA*, 2010.

F. A. Williams. Spray combustion and atomization. *Phys. Fluids*, 1:541–545, 1958.

L.I. Zaichik. A statistical model of particle transport and heat transfer in turbulent shear flows. *Phys. Fluids*, 11: 1521, 1999.

L.I. Zaichik, O. Simonin, and V.M. Alipchenkov. An Eulerian approach for large eddy simulation of particle transport in turbulent flows. *J. Turbul.*, 10(4):1–21, 2009.

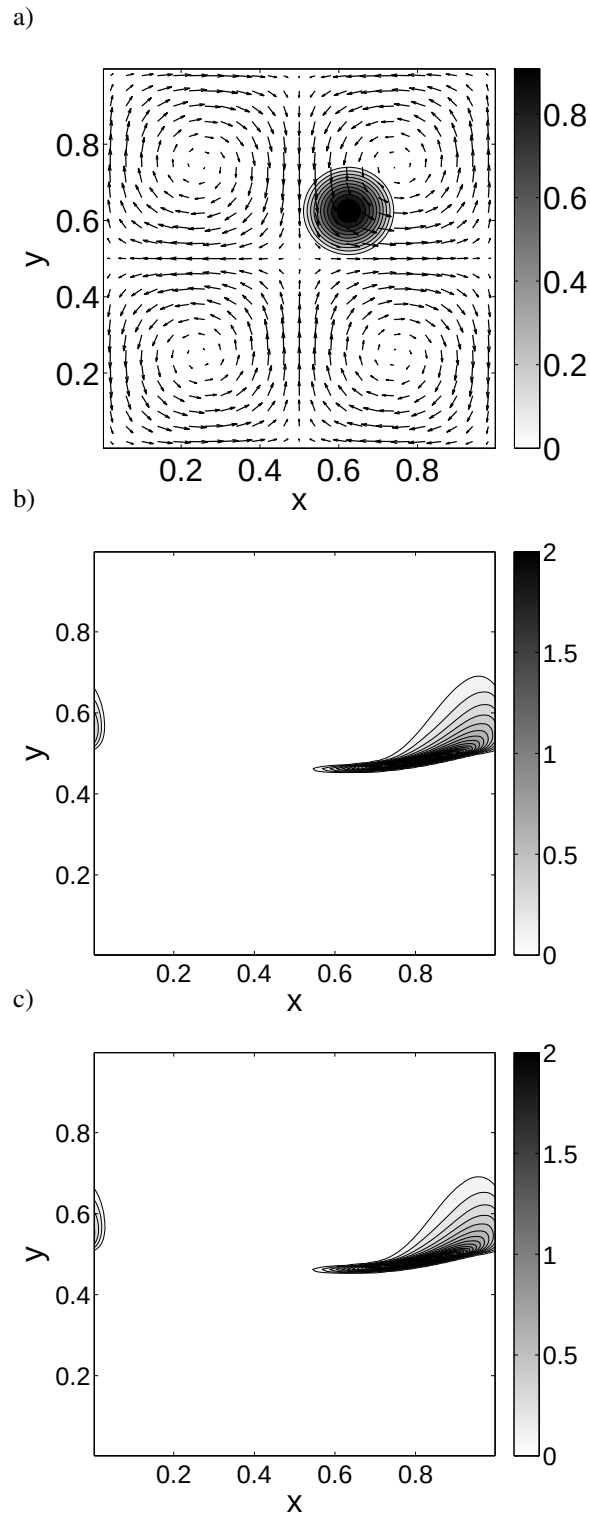

Figure 4: Carrier phase velocity field (Taylor-Green periodic vortices) and initial density contours (a). Snapshots of the density distribution at time $t = 0.8$ for Stokes number $\mathrm{St} = 13\mathrm{St}_c$ (200 nodes, CFL $= 1$): 2nd order Bouchut scheme (b) and 2nd order pressureless relaxation scheme (c).

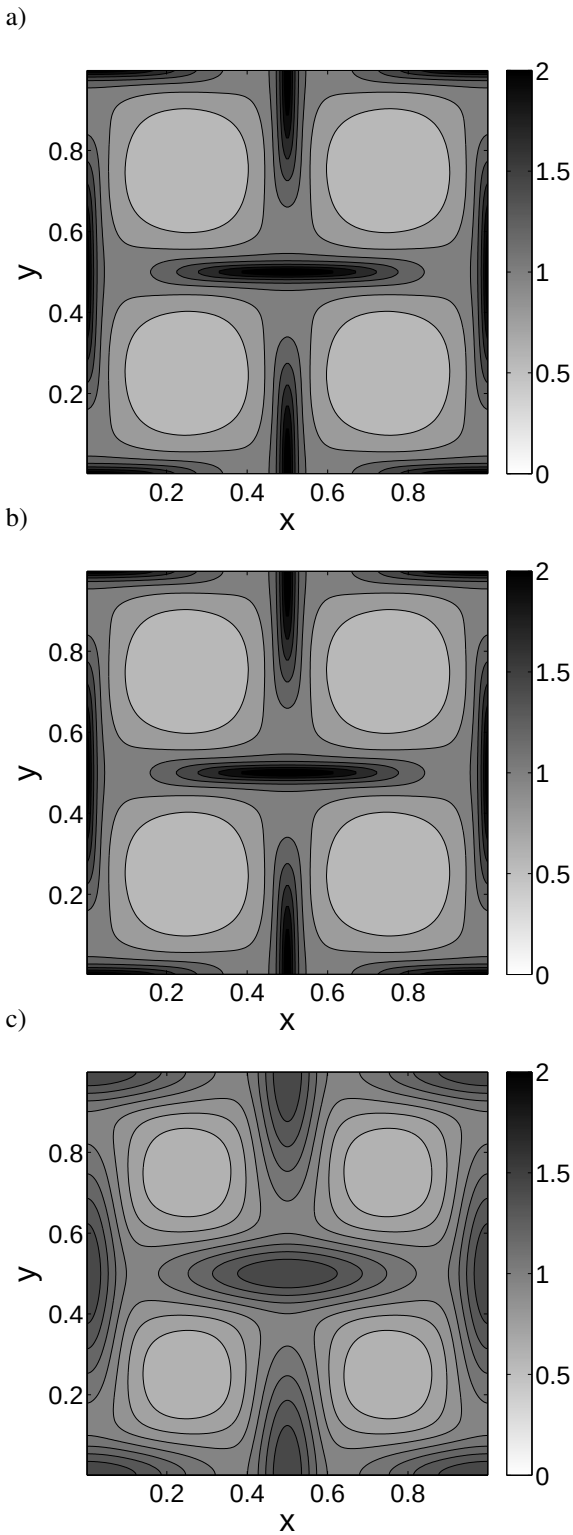

Figure 5: Snapshots of the density distribution at time $t = 0.33$ for Stokes number $\mathrm{St} = 0.9\mathrm{St}_c$: 2nd order Bouchut scheme (a), 2nd order pressureless relaxation scheme (b) and 2nd order relaxation scheme with pressure (c). (a, b): 200 nodes, CFL $= 0.5$. (c): 400 nodes, CFL$=1$.

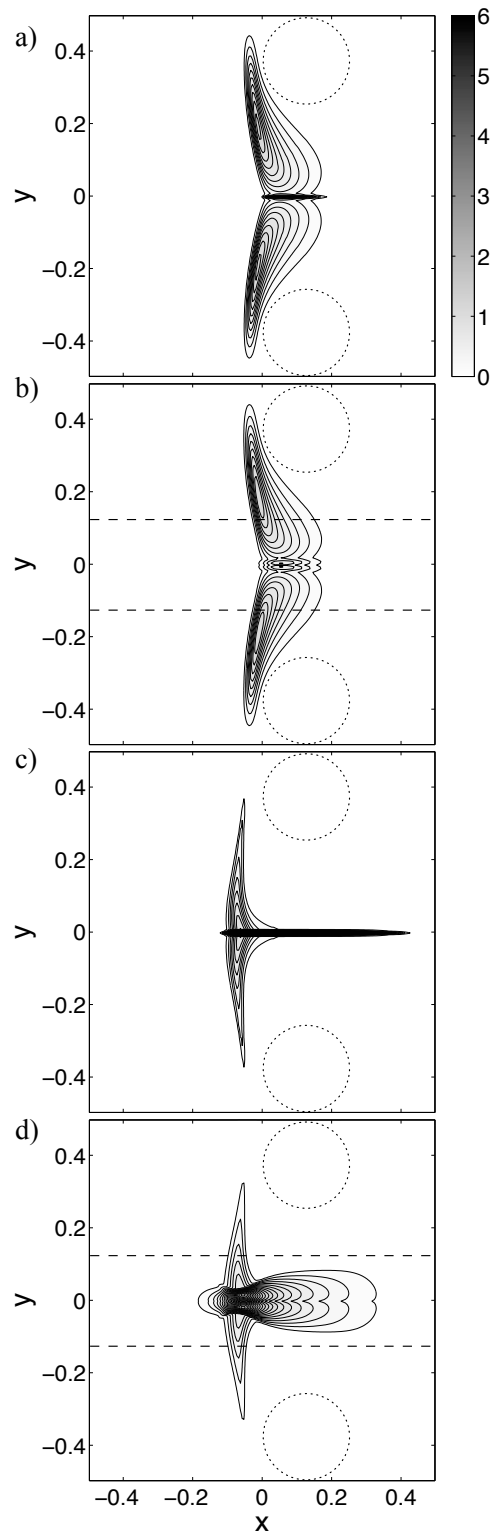

Figure 6: Snapshots of the density for Stokes number $\mathrm{St} = 13\mathrm{St}_c$ (1^{rst} order relaxation scheme, 200 nodes, CFL $= 1$): pressureless scheme (a, c) and hybrid scheme (b, d). Time $t = 0.75$ (a, b) and $t = 1.1$ (c, d). Dotted circles and dashed lines are the limits of the cardinal sinus function of the initial density distribution and the energy source term (b, d) respectively. The maximum density for (c) is 26.81.